Chinese Chemical Letters 33 (2022) 2532–2536

Contents lists available at ScienceDirect

Chinese Chemical Letters

journal homepage: www.elsevier.com/locate/cclet

Structure-fluorescence relationships in pyrrole appended *o*-carborane crystalline materials

Dan Wang[1], Gang Wang[1], Ke Liu, Jing Li, Zhaolong Wang, Jing Liu, Liping Ding, Rong Miao*, Yu Fang

Key Laboratory of Applied Surface and Colloid Chemistry, Ministry of Education, School of Chemistry and Chemical Engineering, Shaanxi Normal University, Xi'an 710062, China

ARTICLE INFO

Article history:
Received 8 August 2021
Revised 3 December 2021
Accepted 9 December 2021
Available online 12 December 2021

Keywords:
Fluorescence
o-Carborane crystal
Steric hinderance
Molecular packing
Temperature sensing

ABSTRACT

Based on three rationally designed pyrrole-appended *o*-carborane derivatives, we present that fluorescence properties of crystalline materials are highly dependent on intermolecular interaction and steric hinderance. Though the three molecules are similar in structure, single crystals of the three compounds showed obvious difference in molecular stacking and fluorescence behavior. Systematic studies indicate that fluorescence quantum yields, thermo-response as well as mechano-response are highly dependent on intermolecular interaction and steric hindrance. In the three crystalline materials, the CB-NMe crystals with weaker intermolecular interaction and looser molecular packing showed superior fluorescence quantum yield and temperature sensitivity. Accordingly, surface temperature detection strip with favorable reversibility is prepared by doping CB-NMe into the polymer. In addition, the CB-NMe aggregates can be used for monitoring bovine serum albumin (BSA) denaturation, as temperature response of the aggregates can be reversed when co-assembled with BSA.

Study on intermolecular packing arrangement-fluorescence property (emission wavelength, quantum yield, environmental sensitivity) relationship in molecular solid-state materials has attracted extensive attention during recent years, owing to the vital roles of these functional materials in sensors, organic light-emitting diodes (OLEDs), solar cells, and *etc.* [1–3]. Different from molecules in solution, molecules in solid state usually exist in their aggregated form. Thus, luminescence behavior of molecular solid is a comprehensive combination of molecular structure, intermolecular interaction, and molecular packing [4–6]. Aggregation caused quenching (ACQ) and aggregation induced emission (AIE) are typical phenomenon to highlight the importance of molecular packing in fluorescent molecular materials [7–10]. In-depth understanding of the structure-function relationship and precise control of intermolecular packing as well as the resulted fluorescence behavior through molecular design lay solid basis for achieving materials with desired performance [11,12].

Up to now, many molecular systems have been designed for understanding solid-state emission and great progress has been achieved in the field [13–16]. Among these, metal complexes, derivatives of typically designed fluorophores are widely used and a series of factors have been proven to be important for their solid-state emissions. For example, emission of the dumbbell-shaped gold(I) molecular rotors is dependent on molecular rotation and aurophilic interactions [17]; fluorescence of perylene diimide-based materials can be tuned by controlling the ratio of *H*-aggregates and *J* aggregates [18]; ACQ feature of some polycyclic aromatic hydrocarbon fluorophores can be avoided when π-π interaction is suppressed [19]. Except for intermolecular interaction, steric hinderance is also important for solid-state fluorescence. Introduction of bulky substitution group can produce anthracene derivative with interesting mechano- and vapo- response [20]. These studies reveal the complexity of solid-state fluorescence, indicating urgent demand for more systematic and in-depth research in the field.

In this study, three pyrrole-substituted *o*-carborane derivatives with similar molecular structure were designed for systematic study on solid-state fluorescence from the point of intermolecular interaction and molecular packing. In the design, *o*-carborane was chosen owing to its electron accepting ability and advantages in fluorescent materials construction [21–23].

Pyrrole, *N*-methylpyrrole, and *N*-phenylpyrrole were included as donor groups and they were linked with aryl-carborane *via* C-C bonds to facilitate their intramolecular rotation [24,25]. Meanwhile, the varied N-terminal substitution from H to bulky groups,

* Corresponding author.
E-mail address: miaorong2015@snnu.edu.cn (R. Miao).
[1] These authors contributed equally to this work.

https://doi.org/10.1016/j.cclet.2021.12.020
1001-8417/

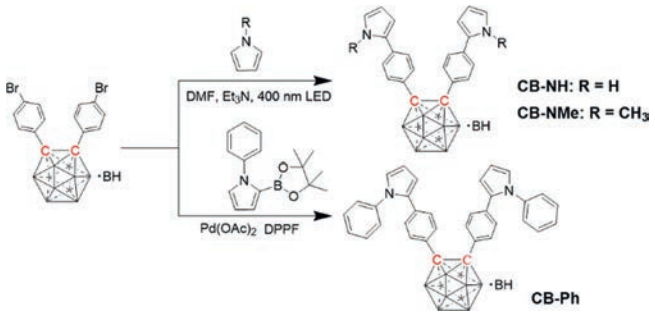

Scheme 1. Synthesis and structures for the *o*-carborane derivatives.

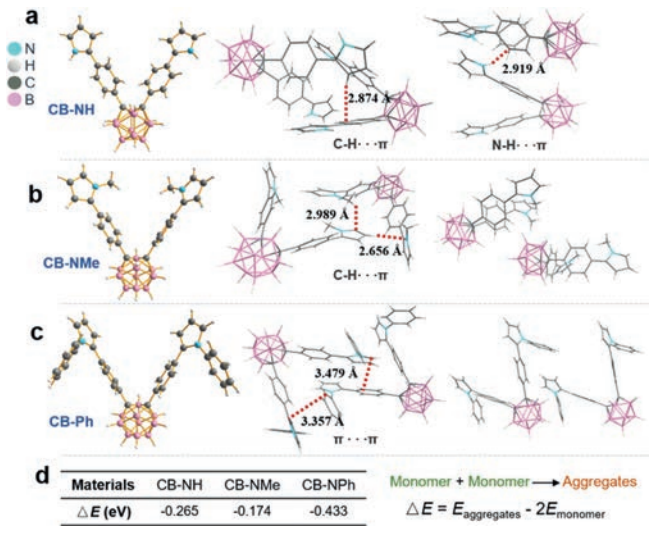

Fig. 1. Refined crystal structures and the representative intermolecular packing of CB-NH (a), CB-NMe (b) and CB-NPh (c). (d) Energy differences between the aggregated molecules and the corresponding monomers.

methyl (CH_3) or phenyl (Ph), would lay foundation for study on both intermolecular interactions and steric hinderance when the molecules aggregate to form crystalline materials. Single crystals of the three compounds were obtained for both structure and fluorescence study; theoretical calculations were done to quantify the strength of intermolecular interaction in the three crystals. What's more, application of the materials in surface temperature indication and protein denaturization were successfully performed.

Synthesis routes of the three compounds are shown in Scheme 1 [24,26,27]. Crystals of the three compounds were obtained by slow evaporation of the compounds in mixture of dichloromethane and *n*-hexane (v/v = 5:1). Structure of the compounds and the corresponding crystals were characterized by ^{1}H NMR, ^{13}C NMR, ESI-MS and X-ray diffractometry (CCDC Nos. 2100344, 2100347 and 2100348).

The X-ray crystallographic results show that the crystals of CB-NH and CB-NMe are monoclinic, while the crystal of CB-Ph (Figs. 1a-c) is triclinic. Intermolecular interaction in the crystals was studied to reveal the substitution effect. Similar to the reported work [28], different types of intermolecular interactions were observed in the three crystals (Fig. 1 and Fig. S1 in Supporting information): N-H···π and C-H···π interactions were observed in CB-NH crystal; C-H···π interaction in CB-NMe crystal; π···π interaction in CB-NPh crystal. To further quantify the intermolecular interaction, energies of each molecule and the corresponding dimer were optimized at the level of M06-2X/6-31G(d,p) based on the X-ray crystal structures (Fig. 1d). Each dimer owned lower energy compared to the monomers. Formation of the dimer led to 0.265, 0.174 and 0.433 eV reductions in energy for CB-NH, CB-NMe and CB-NPh respectively, demonstrating the influence of *N*-terminal substitution on molecular packing.

Based on the structure study, photophysical behaviors of the three compounds were studied. UV-vis spectra were recorded (Figs. S2–S5 in Supporting information). The three compounds showed similar absorption around 230 and 311 nm, which should be attributed to π-π^* transitions and charge transfer transitions [29]. In the experiment, we found that the three crystals were highly fluorescent, while the solutions were nonfluorescent, suggesting AIE characteristic of the compounds. Fluorescence emission spectra of the crystals are shown in Fig. 2a. It can be seen that the three crystals showed similar feature in both emission and excitation spectrum. In accordance with the theoretical calculations (Fig. S6 in Supporting information) and UV-vis studies (Fig. S5), the three crystals showed fluorescence of charge transfer characteristic with large stocks shifts of ~250 nm. AIE responses of the compounds were studied by measuring fluorescence emission spectrum of the compound in the mixture of tetrahydrofuran (THF) and water (Fig. 2b). Each system showed turn on fluorescence when volume fraction of water exceeded 80% (Fig. 2c). Fluorescence lifetime and absolute fluorescence quantum yields (QY) of the three crystals were also measured (Fig. 2d). The CB-NMe crystal showed the highest QY of 63.4% with a lowest lifetime of 4.62 ns.

Fluorescence of solid materials is highly dependent on the motion and configuration, thus we tried to investigate the responses of the fluorescent crystals to heating and mechanical grinding. Both the three crystals and aggregated dispersions showed decreased fluorescence intensity upon temperature increasing (Fig. 3a, Figs. S7–S9 in Supporting information), which suggests the increased non-radiative passway as a result of activated molecular movement. Further inspection of the response dynamics reveals that the three crystals had different quenching efficiency upon heating. Fluorescence of the CB-NPh crystal only decreased 30.0% when the temperature was increased from 25 °C to 115 °C. Nevertheless, the CB-NMe crystal showed the highest quenching efficiency (55.4%) and best linear relationship (R^2 = 0.9992) between fluorescence intensity and temperature (Fig. 3b). Meanwhile, fluorescence lifetime of the CB-NMe crystal gradually decreased from 4.62 ns to 2.82 ns during the heating process (Fig. 3c).

It was also interesting to find that the CB-NPh crystal exhibited opposite fluorescence response to mechanical griding in comparison to CB-NH or CB-NMe crystal (Fig. S10 in Supporting information). The CB-NH crystal and CB-NMe crystal showed red-shifts (15 and 12 nm) after griding, while the CB-NPh exhibited a blue shift (14 nm). UV-vis absorption spectra were also recorded to understand the aggregation behavior (Fig. S11 in Supporting information). The absorption spectra of CB-NH and CB-NMe were broadened and red-shifted after griding, while the CB-NPh showed narrowed and blue-shifted absorption. The results indicated that the CB-NH or CB-NMe molecules were less loosely packed in the crystals than in the grounded powders, while the CB-NPh is different owing to larger steric hinderance of the phenyl group [30].

The results from photophysical behavior study consolidate the significant influence of *N*-terminal substitution. Reasons from two aspects can be used to explain the difference in fluorescence responses to heating and grinding: intermolecular interaction and steric hindrance. Referring to the theoretical calculations in Fig. 1d and the effect of steric hinderance (Ph > Me > H), it is easy to understand the fluorescence behavior of the three crystals. The highest quantum yield and superior temperature response of the CB-NMe crystal could be resulted from the weakly constrained molecules, where nonradiative pathway aroused from tight intermolecular overlapping can be reduced [18].

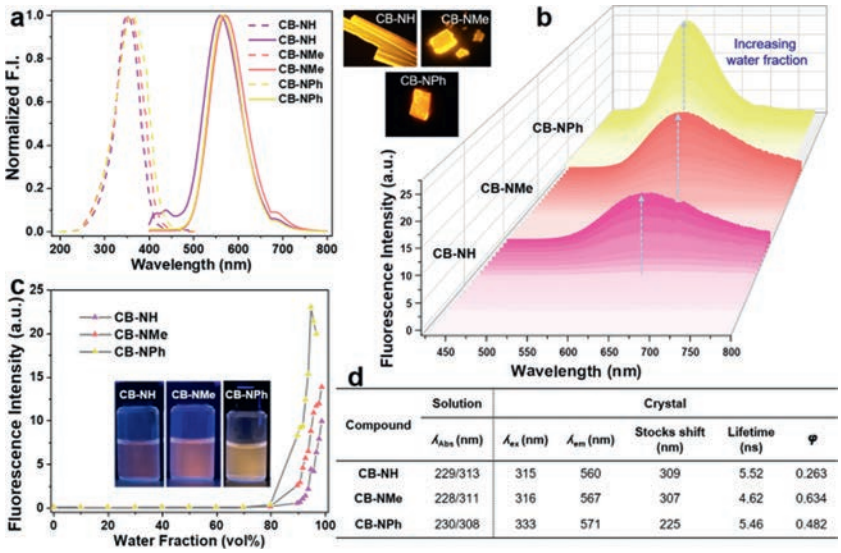

Compound	Solution	Crystal				
	λ_{Abs} (nm)	λ_{ex} (nm)	λ_{em} (nm)	Stocks shift (nm)	Lifetime (ns)	φ
CB-NH	229/313	315	560	309	5.52	0.263
CB-NMe	228/311	316	567	307	4.62	0.634
CB-NPh	230/308	333	571	225	5.46	0.482

Fig. 2. (a) Normalized fluorescence excitation (dashed) and emission (solid) spectra of the crystals. Inset: fluorescence image of the crystals. (b) Fluorescence emission spectra of CB-NH, CB-NMe and CB-NPh in THF/H_2O mixtures. (c) Fluorescence intensity of CB-NH, CB-NMe and CB-NPh suspension as a function of water fraction. (d) Photophysical properties of the molecules.

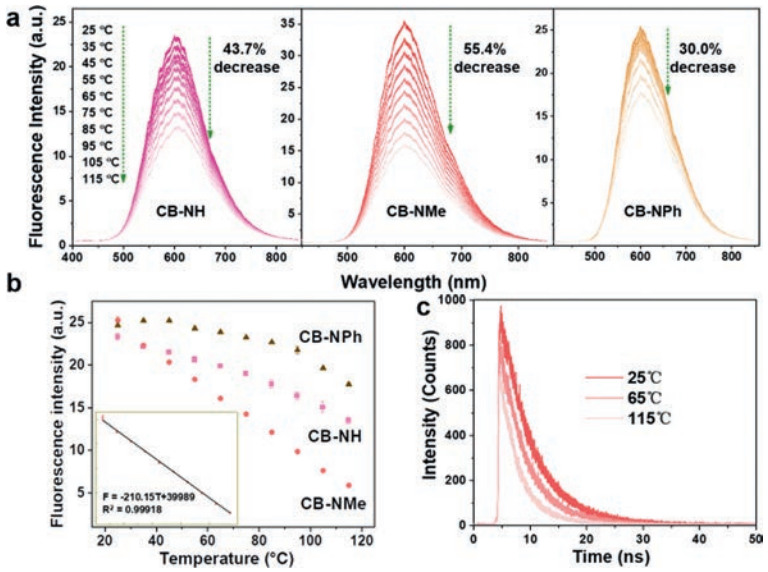

Fig. 3. (a) Fluorescence emission spectra of the crystals at varied temperatures. (b) Fluorescence intensity of each crystal as a function of temperature. (c) Fluorescence lifetime of the CB-NMe crystal under different temperatures.

Based on the understanding, applications of the fluorescent materials were explored using CB-NMe. For reliable and user-friendly surface temperature monitoring strip, CB-NMe was dopped into thermoplastic polymer styrene-ethylene/butylene-styrene (SEBS). At ambient temperature, the polymer was transparent, but it was highly fluorescent under UV light (Fig. 4a). Similar to CB-NMe crystal, fluorescence of the polymer gradually decreased upon temperature increasing. There is good linear relationship ($R^2 = 0.9976$) between fluorescence intensity of the strip and temperature (Fig. 4b). Little response fade was found after 5 cycles, indicating favorable reusability. Meanwhile, the change can be visualized (Fig. 4c), especially when the temperature rose to 55 °C. A color card was made by extracting the RGB values of the fluorescence images under different temperatures. Therefore, surface temperature of a targeted object can be visualized. For practical test, surface temperature of computer host and refrigerator were estimated. Comparing with the color card, the highest surface temperature of the refrigerator (side position near the motor) and computer host could be in the range of 40∼55 °C and 55∼70 °C, respectively. The results went well with the thermal effect of central process unit (CPU) and compressor during their smooth running.

In addition, CB-NMe can be used to monitor protein denaturization when co-assembled with BSA, which is usually used as carrier protein because of its favorable hydrophobic pocket [31]. The emission spectra of aggregated CB-NMe molecules showed gradual shift to shorter wavelength upon the increasing of BSA concentration (Figs. S12 and S13 in Supporting information). Fluorescence intensity of the CB-NMe aggregates exhibited an increase of almost 4 times with a blue shift of 44 nm upon the introducing of BSA into the system, inferring the interaction between the aggregated CB-NMe and BSA (Fig. 4d). Temperature response of the CB-NMe/BSA system was also inspected (Fig. 4e and Fig. S14 in Supporting information). It was interesting to find that temperature response of the

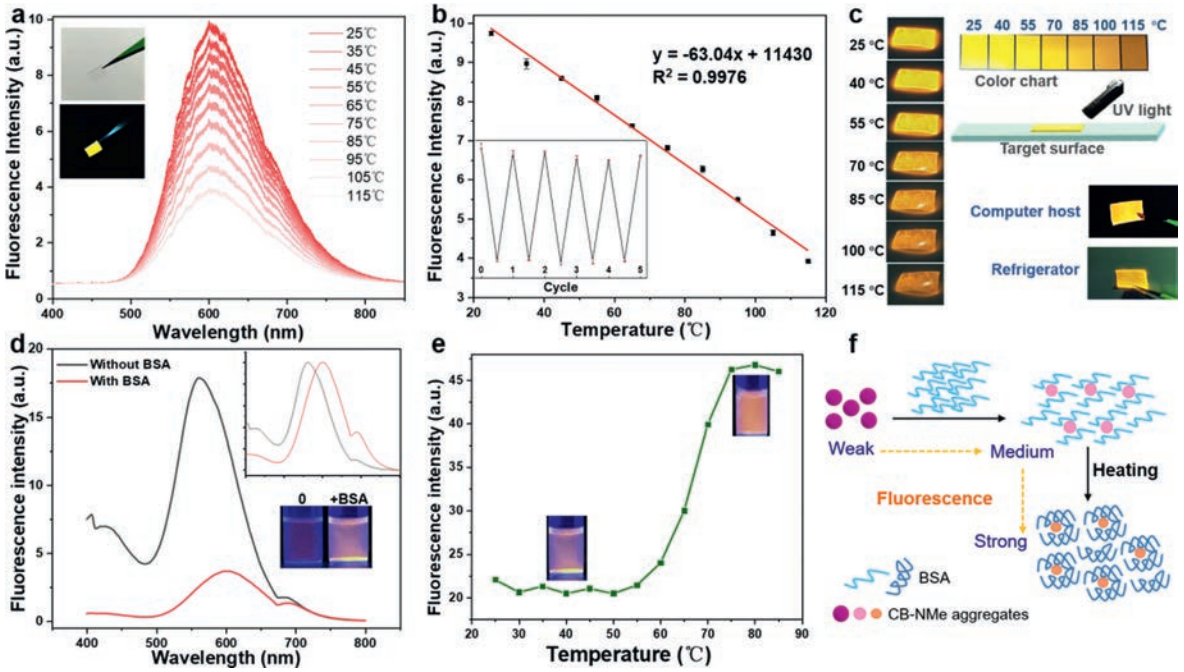

Fig. 4. (a) Fluorescence spectra of the strip under different temperatures. Inset: The strip under sunlight and 365 nm UV light. (b) Fluorescence intensity of the strip as a function of temperature. Inset: Reversible response of the strip in temperature sensing. (c) Fluorescence images of the strip at different temperatures and the application. (d) Fluorescence spectra of CB-NMe aggregates with/without BSA. Inset: Normalized fluorescence spectra and the fluorescence images of the solution. (e) Fluorescence intensity of CB-NMe/BSA as a function of temperature and the corresponding fluorescence images. (f) Proposed interaction between CB-NMe aggregates and BSA.

CB-NMe/BSA system was totally different from the CB-NMe aggregates. It can be noticed that the temperature response range (55–75 °C) of the system matched well with the denaturization temperature of BSA [32], which not only consolidate the interaction between CB-NMe aggregates and BSA but also indicates the ability of the CB-NMe in protein denaturization monitoring. To elucidate the interaction between CB-NMe aggregates and BSA, dynamic light scattering (DLS) was used (Fig. S15 in Supporting information). The DLS results showed that introduction of BSA resulted in decrease in hydrodynamic diameter of CB-NMe aggregates, especially when the mixture was heated. Based on the result, a plausible mechanism is proposed to understand the interaction between CB-NMe aggregates and BSA (Fig. 4f). Smaller CB-NMe aggregates with enhanced and blue shifted emission were formed owing to the interaction between CB-NMe aggregates and BSA. Upon the denaturization of BSA, hydrophobic pockets were exposed, which promoted the interaction between CB-NMe and BSA, therefore, the CB-NMe/BSA aggregates became smaller and much more fluorescent.

In conclusion, three *o*-carborane derivatives were typically designed for systematic study on structure-fluorescence relationship in crystalline materials. Variation in pyrrole groups endows the three compounds different intermolecular interaction and steric hinderance in their corresponding crystalline materials. Combined with single crystal diffraction results, photophysical properties of the three molecular materials have been comprehensively studied, including AIE behavior, thermal response, and mechanical response. Based on the study, it can be concluded that stronger intermolecular interaction could result in lower fluorescence quantum yield in solid state materials, even though for AIEgens. Because of its favorable thermal response, CB-NMe was dopped into SEBS to make a temperature sensing strip for fast and reversible visualization of surface temperature. What's more, temperature response of CB-NMe aggregates could be dramatically changed when BSA was introduced, which offers a reliable way for monitoring BSA denaturization.

Declaration of competing interest

The authors report no declarations of interest.

Acknowledgments

We acknowledge the funding from the Natural Science Foundation of China (Nos. 22072084, 21820102005), 111 Project (No. B14041), the Fundamental Research Funds for the Central Universities (Nos. GK202103048, GK202001005, 2020CSLY008), and the Innovation Capability Support Program of Shaanxi (No. 2021TD-18).

Supplementary materials

Supplementary material associated with this article can be found, in the online version, at doi:10.1016/j.cclet.2021.12.020.

References

[1] X.D. Wang, O.S. Wolfbeis, R.J. Meier, Chem. Soc. Rev. 42 (2013) 7834–7869.
[2] J. Guo, X.L. Li, H. Nie, et al., Chem. Mater. 29 (2017) 3623–3631.
[3] H. Liu, N. Ando, S. Yamaguchi, et al., Chin. Chem. Lett. 32 (2021) 1669–1674.
[4] D. Bialas, E. Kirchner, M.I.S. Rohr, et al., J. Am. Chem. Soc. 143 (2021) 4500–4518.
[5] J. Gierschner, J. Shi, B. Milián-Medina, et al., Adv. Opt. Mater. 9 (2021) 2002251.
[6] Z. Ma, Y. Ji, Y. Lan, et al., J. Mater. Chem. C 6 (2018) 2270–2274.
[7] F. Wurthner, Angew. Chem. Int. Ed. 59 (2020) 14192–14196.
[8] J. Guan, C. Shen, J. Peng, et al., J. Phys. Chem. Lett. 12 (2021) 4218–4226.
[9] J. Mei, N.L. Leung, R.T. Kwok, et al., Chem. Rev. 115 (2015) 11718–11940.
[10] J. Sturala, M.K. Etherington, A.N. Bismillah, et al., J. Am. Chem. Soc. 139 (2017) 17882–17889.
[11] Y. Gong, S. He, Y. Li, et al., Adv. Opt. Mater. 8 (2020) 1902036.
[12] Q. Li, Z. Li, Acc. Chem. Res. 53 (2020) 962–973.
[13] J. Wang, Y. Yu, L. Niu, et al., Chem. Commun. 56 (2020) 6269–6272.
[14] X. Ma, W. Chi, X. Han, Chin. Chem. Lett. 32 (2021) 1790–1794.
[15] I.D.W. Samuel, G.A. Turnbull, Chem. Rev. 107 (2007) 1272–1295.
[16] P. Chen, J. Wang, L. Niu, et al., J. Mater. Chem. C 5 (2017) 12538–12546.
[17] M. Jin, T.S. Chung, T. Seki, M.A. Garcia-Garibay, et al., J. Am. Chem. Soc. 139 (2017) 18115–18121.
[18] N.J. Hestand, F.C. Spano, Chem. Rev. 118 (2018) 7069–7163.
[19] Y. Huang, J. Xing, Q. Gong, et al., Nat. Commun. 10 (2019) 169.
[20] Y. Matsunaga, J.S. Yang, Angew. Chem. Int. Ed. 54 (2015) 7985–7989.

[21] K. Nishino, H. Yamamoto, K. Tanaka, et al., Org. Lett. 18 (2016) 4064–4067.
[22] K. Kokado, Y. Chujo, J. Org. Chem. 76 (2011) 316–319.
[23] H. Naito, Y. Morisaki, Y. Chujo, Angew. Chem. Int. Ed. 54 (2015) 5084–5087.
[24] R. Miao, J. Li, Z. Luo, et al., J. Chem. Educ. 97 (2020) 4469–4474.
[25] Y. Haketa, M. Miyasue, Y. Kobayashi, et al., J. Am. Chem. Soc. 142 (2020) 16420–16428.
[26] T. Han, J. Yang, R. Miao, et al., Adv. Mater. Technol. 6 (2021) 2000933.
[27] R. Miao, D. Wang, J. Xiao, et al., Phys. Chem. Chem. Phys. 22 (2020) 10212–10218.
[28] N.V. Nghia, S. Jana, S. Sujith, et al., Angew. Chem. Int. Ed. 57 (2018) 12483–12488.
[29] D.K. You, H. So, C.H. Ryu, et al., Chem. Sci. 12 (2021) 8411–8423.
[30] M. Hecht, F. Würthner, Acc. Chem. Res. 54 (2021) 642–653.
[31] V.S. Jisha, K.T. Arun, M. Hariharan, et al., J. Am. Chem. Soc. 128 (2006) 6024–6025.
[32] X. Liu, W. Zhang, J. Liu, et al., Food Hydrocoll. 101 (2020) 105450.